JACS Au
AN OPEN ACCESS JOURNAL OF THE AMERICAN CHEMICAL SOCIETY

pubs.acs.org/jacsau

Article

# Fluorescein-Based Type I Supramolecular Photosensitizer via Induction of Charge Separation by Self-Assembly

Hajime Shigemitsu,* Kei Ohkubo, Kazuhide Sato, Asuka Bunno, Tadashi Mori, Yasuko Osakada, Mamoru Fujitsuka, and Toshiyuki Kida*

Cite This: *JACS Au* 2022, 2, 1472−1478

Read Online

ACCESS | Metrics & More | Article Recommendations | Supporting Information

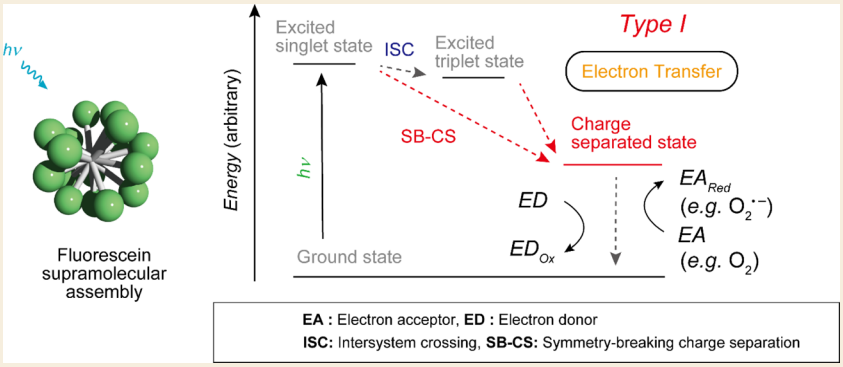


**ABSTRACT:** Photosensitizers (PSs) are critical substances with considerable potential for use in non-invasive photomedicine. Type I PSs, which generate reactive radical species by electron transfer from the excited state induced via photoirradiation, attracted much attention because of their suitability for photodynamic therapy (PDT) irrespective of the oxygen concentration. However, most organic PSs are type II, which activates only oxygen, generating singlet oxygen ($^1O_2$) via energy transfer from the triplet state. Here, we proposed a strategy to form type I supramolecular PSs (SPSs) utilizing the charge-separated state induced by self-assembly. This was demonstrated using a supramolecular assembly of fluorescein, which is a type II PS in the monomeric state; however, it changes to a type I SPS via self-assembly. The switching mechanism from type II to I via self-assembly was clarified using photophysical and electrochemical analyses, with the type I SPS exhibiting significant PDT effects on cancer cells. This study provides a promising approach for the development of type I PSs based on supramolecular assemblies.

**KEYWORDS:** *supramolecular assembly, fluorescein, type I photosensitizer, reactive oxygen species (ROS), charge separation*

## 1. INTRODUCTION

Photodynamic therapy (PDT) is a promising approach for treating cancer and microbial infections.[1−3] The photosensitization reaction in PDT proceeds only in the region irradiated with light, generating reactive oxygen species (ROS) and radical species.[4] As the chemical process occurs within a few tens of nanometers, PDT exhibits spatiotemporal selectivity and is minimally invasive. However, due to the lack of an ideal photosensitizer (PS) and methods of selective transport and/or activation at the disease site, PDT is only applied in treating a limited number of diseases.[5,6] One of the problems is the low PDT efficiency toward cancer cells.[7,8] Most PSs proceed with type II photosensitization reactions that activate only oxygen, generating $^1O_2$ via energy transfer from the triplet state. Type II PDT is oxygen-dependent and thus ineffective for cancer cells under hypoxic conditions.[9] Cancer cells exhibit significantly high proliferative capacities and use excessive amounts of oxygen, resulting in a hypoxic microenvironment surrounding the tumor.[10] Therefore, PSs enabling PDT under hypoxic conditions are required. In contrast to type II PSs, type I PSs generate various active radical species [e.g., superoxide ($O_2^{\bullet-}$), hydroxy radical ($^{\bullet}$OH)] via electron transfer from the excited state even in a hypoxic environment and hence exhibit potential for non-oxygen-dependent PDT.[11] Therefore, research regarding the development of type I PSs has accelerated.[12−15]

Supramolecular assemblies are of considerable interest in the field of nanomedicine because they may be prepared using facile "bottom-up" methods and tuned at the molecular level.[16−19] Nano-sized supramolecular assemblies, such as porphyrin-peptide assembled nanodots[20] and pillararene,[21]

Received: April 19, 2022
Revised: May 12, 2022
Accepted: May 13, 2022
Published: May 24, 2022





https://doi.org/10.1021/jacsau.2c00243
*JACS Au* 2022, 2, 1472−1478

demonstrated the potential in photomedicine. Numerous supramolecular assemblies based on small molecules were designed to overcome the various limitations of PDT.[22−29] These materials exhibit cancer-selective, biocompatible, and light-absorbing properties due to the molecular-level design of the constituents and functional molecule hybridization via non-covalent bonds. However, type I supramolecular PSs (SPSs) are still rare. To the best of our knowledge, there is only one method for their preparation. Yoon and co-workers showed that phthalocyanines with electron-donating amine groups self-assembled to function as type I SPSs.[30] The proximity of the electron-donating group to the triplet state PS enables rapid reductive quenching, yielding a radical anion that induces electron transfer to oxygen or substrates. Therefore, the hybridization of PSs and electron-donating groups may give type I SPSs.[31−33] However, this strategy requires the introduction of electron-donating substituents onto the PS backbone, which may result in a complex synthesis and challenges in further functionalization. The development of another method for producing a type I SPS without such limitations may result in more efficient PDT.

In this study, we proposed a simple strategy to prepare a type I SPS via a charge-separated (CS) state of a PS and showed that fluorescein which is a type II PS in the monomeric state changes to a type I SPS via self-assembly (Figure 1). The CS state induced by self-assembly is crucial for the generation of a type I SPS. Generally, in the excited triplet states of organic molecules, type II photosensitization reactions proceed preferentially. We assumed that if the CS state, which is prone to electron transfer, is somehow stabilized over the triplet state, the type II reaction is suppressed, and the type I reaction preferentially proceeds (Figure 1). Inspired by our previous studies of rhodamine and cyanine dyes forming a CS state via self-assembly and acquiring photosensitizing function,[34,35] we speculated that in various molecules, CS states could be stabilized in the self-assembly states. Furthermore, certain type II organic PSs could be transformed into type I SPSs via self-assembly. In fact, the supramolecular assembly of fluorescein, which is a typical type II PS in the monomer state, functions as a type I PS (Figure 1) exhibiting significant PDT effects on cancer cells.

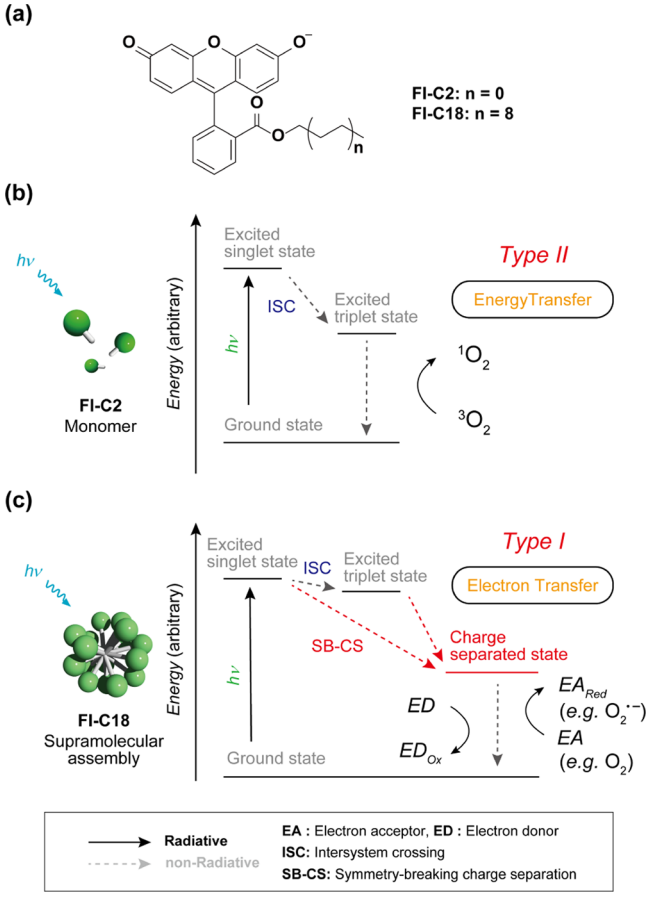


**Figure 1.** (a) Chemical structures of **Fl-C2** and **Fl-C18**. (b,c) (b) Type II and (c) Type I photosensitization mechanisms of (b) **Fl-C2** (monomer state) and (c) **Fl-C18** (assembly state), respectively. The radiative decay processes from excited states are omitted for clarity.

## 2. RESULTS AND DISCUSSION

### 2.1. Self-Assembly Properties of Fluoresceins

Fluorescein was used as a representative constituent of a type I SPS (Figure 1a). It is a typical fluorescent dye used as a chemical probe.[36,37] Fluoresceins generally exhibit type II photosensitizing functions and are used in chromophore-assisted light inactivation.[38,39] The energy level of the CS state of fluorescein may be lower than that of the $T_1$ state, and the CS state can be generated by symmetry-breaking charge separation (SB−CS) and charge carrier migration in the assembly.[40] Amphiphilic **Fl-C18** was synthesized to form the self-assembly of fluorescein in water (Figure 1a and Scheme S2). For comparison, hydrophilic **Fl-C2**, with a short ethyl chain, was also synthesized (Scheme S1). The absorption and fluorescence spectra of **Fl-C2** and **Fl-C18** in the monomer state in dimethyl sulfoxide (DMSO) revealed that **Fl-C2** and **Fl-C18** are suitable for evaluating the changes in photophysical properties via self-assembly in water. The absorption and fluorescence spectra of **Fl-C2** and **Fl-C18** are almost identical [Figure S1, $\lambda_{abs}$: 530 (**Fl-C2**) and 531 (**Fl-C18**) nm, $\lambda_{em}$: 556 (**Fl-C2**) and 556 (**Fl-C18**) nm], indicating that the difference in alkyl chain length hardly affects the photophysical properties.

To evaluate the self-assembly properties in water, absorption and fluorescence spectra were measured (Figure 2a,b). The absorption spectrum of **Fl-C2** exhibits a similar shape to that in DMSO ($\lambda_{abs}$: 494 nm) whereas that of **Fl-C18** reveals a decrease in absorbance, with the maximal absorption band split and broadening ($\lambda_{abs}$: 508 nm). This splitting is due to the H- and J-type fluorescein aggregate mixtures,[41] and the broadening suggests random aggregation. The fluorescence of **Fl-C18** is significantly lower than that of **Fl-C2** [$\lambda_{em}$: 520 (**Fl-C2**) and 517 (**Fl-C18**) nm], with quantum yields of 0.75 and 0.008 for **Fl-C2** and **Fl-C18**, respectively. The average aggregate size of **Fl-C18** determined by dynamic light scattering (DLS) is 103 nm, and transmission electron microscopy (TEM) observation reveals the formation of spherical aggregates (Figure 2c,d).

### 2.2. ROS Generation by Fl-C2 and Fl-C18

The photosensitizing functions of **Fl-C2** and **Fl-C18** were evaluated using ROS detection probes such as 9,10-anthracenediyl-bis(methylene)-dimalonic acid (**ABDA**)[42] and dihydrorhodamine 123 (**DHR123**)[43] (Figure S2). First, we performed studies using **ABDA** to detect singlet oxygen ($^1O_2$) produced by energy transfer from the PS to molecular oxygen (type II photosensitization reaction). Light irradiation (460


https://doi.org/10.1021/jacsau.2c00243
JACS Au 2022, 2, 1472−1478

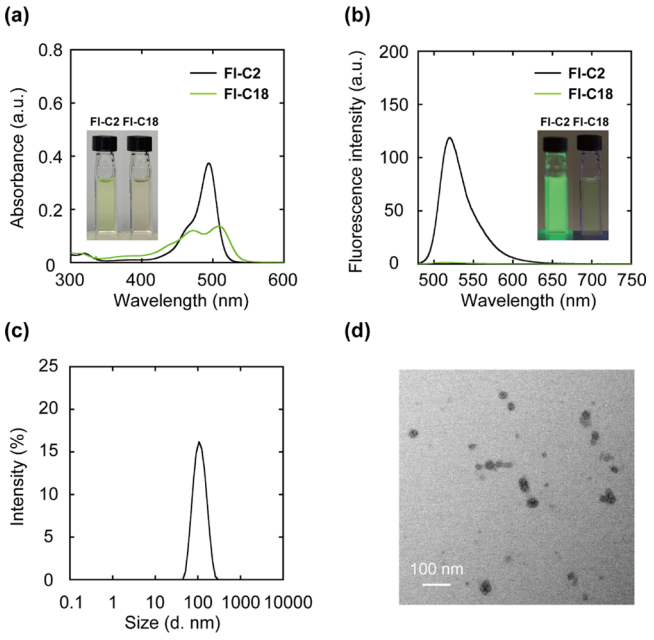


**Figure 2.** (a) UV−vis and (b) PL spectra of **Fl-C2** and **Fl-C18**. Experimental conditions: [**Fl-C2**] = [**Fl-C18**] = 5.0 $\mu$M, 1.0 mM phosphate buffer solution, rt, excitation wavelength: 460 nm. (c) Size distribution of the supramolecular assembly of **Fl-C18** determined using DLS (*Z*-average: 103 nm, PDI: 0.10). (d) TEM image of the **Fl-C18** supramolecular assemblies. Experimental conditions: [**Fl-C2**] = [**Fl-C18**] = 1.0 $\mu$M, 1.0 mM phosphate buffer solution, rt.

nm, 300 W, Xe lamp) of the **Fl-C2**/**ABDA** mixture results in a time-dependent decrease in the fluorescence intensity of **ABDA**, suggesting that monomeric **Fl-C2** functions as a type II PS (Figure 3a). Time-dependent decrease in fluorescence

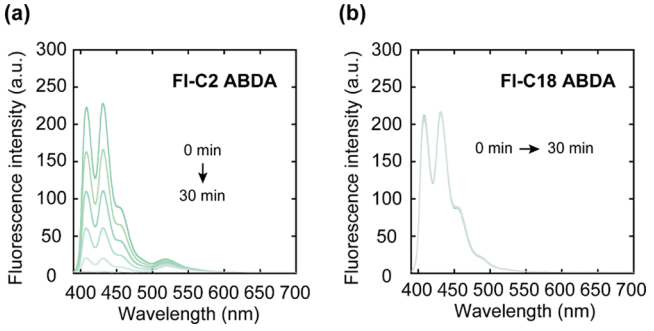


**Figure 3.** Fluorescent spectra of the mixtures after photoirradiation ($\lambda_{ex}$: 360 nm). (a) **Fl-C2** and **ABDA** and (b) **Fl-C18** and **ABDA**. Experimental conditions: [**Fl-C2**] = [**Fl-C18**] = [**ABDA**] = 5.0 $\mu$M, 1.0 mM phosphate buffer solution, rt. Irradiation light: 460 nm, 300 W, Xe lamp.

intensity of **ABDA** did not occur without the **Fl** derivatives (Figure S3). The generation of $^1O_2$ by **Fl-C2** was also confirmed by phosphorescence emission of $^1O_2$ ($\lambda_{em}$: 1270 nm) (Figure S4). Conversely, there is no decrease in the fluorescence intensity of **ABDA** with **Fl-C18** (Figure 3b). The residual ratios of **ABDA** after 30 min photoirradiation are <0.01 and 1.0 for **Fl-C2** and **Fl-C18**, respectively (Figure S5). These results indicate that the type II photosensitization reaction of **Fl-C18** is almost suppressed. Subsequently, the ROS generated by **Fl-C18** were examined using **DHR123**, which converts to emissive rhodamine 123 (**Rh123**) upon oxidation (Figure S2b) and superoxide dismutase (SOD),[44] which is a quencher of superoxide ($O_2^{\bullet-}$) generated by type I photosensitization. As shown in Figure S6a,c,e, with **Fl-C2**, there is no change in the increasing **Rh123** fluorescence intensity regardless of the presence of SOD. Conversely, with **Fl-C18**, the rate of increase in the fluorescence intensity of **Rh123** is slightly decreased (Figure S6b,d,f), suggesting that **Fl-C18** generates superoxides in an aqueous solution via a type I photosensitization reaction. In addition, to confirm the generation of $O_2^{\bullet-}$ by **Fl-C18**, we examined the reduction of cytochrome *c* by photoirradiation (Figure S7). It is known that cytochrome *c* is reduced by $O_2^{\bullet-}$ to afford reduced cytochrome *c* whose characteristic absorption band is at 550 nm.[45] After photoirradiation to the mixture of **Fl-C18** and cytochrome *c*, the absorption band at 550 nm was increased ($\Delta A_{550nm}$: 0.11). However, under the existence of SOD, the absorption band intensity was hardly changed ($\Delta A_{550nm}$: 0.04). These results support the $O_2^{\bullet-}$ generation via **Fl-C18**.

Electron spin resonance (ESR) spectroscopy was performed using spin-trapping reagents 4-hydroxy-2,2,6,6-tetramethylpiperidine (**4-OH-TEMP**)[46] and 1-hydroxy-3-carboxy-2,2,5,5-tetramethylpyrrolidine (**CPH**)[47] to examine $^1O_2$ and $O_2^{\bullet-}$ generation. **4-OH-TEMP** and **CPH** react with $^1O_2$ or $O_2^{\bullet-}$ to generate ESR-detectable 4-hydroxy-2,2,6,6-tetramethylpiperidine 1-oxyl (**4-OH-TEMPO**) and CP (**CP$^\bullet$**) radicals, respectively (Figure S8). Figure 4a displays the ESR spectra

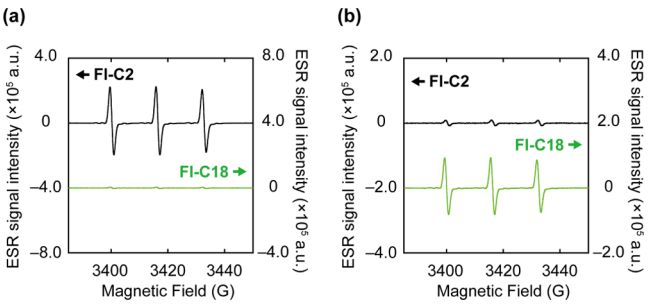


**Figure 4.** ESR spectra of the mixtures with spin-trapping reagents after photoirradiation. (a) **4-OH-TEMP** or (b) **CPH** with **Fl-C2** (upper) or **Fl-C18** (lower). Experimental conditions: [**Fl-C2**] = [**Fl-C18**] = 5.0 $\mu$M, [**4-OH-TEMP**] = [**CPH**] = 50 $\mu$M, 1.0 mM phosphate buffer solution, rt.

of **Fl-C2**/**4-OH-TEMP** and **Fl-C18**/**4-OH-TEMP** mixtures after 1 min of photoirradiation, which show clear and no ESR signals, respectively. Therefore, **Fl-C2** generates $^1O_2$ after photoirradiation, but **Fl-C18** does not. Subsequently, we examined the spin-trapping reagent **CPH** for $O_2^{\bullet-}$ detection. The distinct triplet ESR signal of **CP$^\bullet$** is observed for the **Fl-C18**/**CPH** mixture after photoirradiation (Figure 4b). The supramolecular assembly of **Fl-C18** promotes electron transfer to molecular oxygen, and the CS state would be generated. The ESR spectra are consistent with the results obtained using the ROS chemical probes. Therefore, the photosensitization mechanism of fluorescein is clearly altered by self-assembly.

### 2.3. Mechanistic Study of Self-Assembly-Induced Switching of ROS Generation

Nanosecond laser flash photolysis was performed to elucidate the mechanistic details of the **Fl-C2** and **Fl-C18** photosensitizing reactions.[48] The nanosecond transient absorption (TA) spectra of **Fl-C2** and **Fl-C18** were measured after nanosecond laser excitation at 460 nm in a deaerated aqueous buffer


https://doi.org/10.1021/jacsau.2c00243
JACS Au 2022, 2, 1472−1478

solution (Figure S9). For **Fl-C2**, a TA band at 550 nm with a relatively long lifetime ($t_{1/2}$ = 7.2 $\mu$s) is observed (Figure 5a),

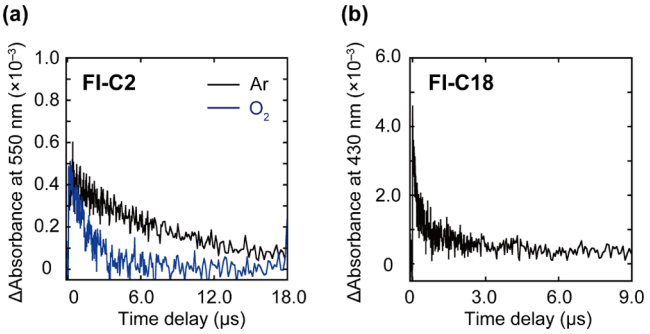


**Figure 5.** TA decay profiles of (a) **Fl-C2** and (b) **Fl-C18** at (a) 550 and (b) 430 nm. (a) Black and blue lines are TA decay profiles under Ar and $O_2$ atmospheres, respectively. Experimental conditions: [**Fl-C2**] = 50 $\mu$M, [**Fl-C18**] = 100 $\mu$M, 1.0 mM phosphate buffer solution (pH 7.4), rt. Excitation light: 460 nm.

and the lifetime is significantly shortened in the presence of oxygen ($t_{1/2}$ = 1.1 $\mu$s), which is attributed to the triplet state of **Fl-C2**.[49,50] Conversely, the spectrum of **Fl-C18** showed no TA band at 550 nm (Figure S10a). Instead of triplet formation, the spectrum of **Fl-C18** exhibits a new TA band at 430 nm (Figure 5b), which is not observed for **Fl-C2** (Figure S10b). The lifetime (>10 $\mu$s) is sufficient for chemical reactions, and the transient species may be in a CS state involving the photoreaction. The signal is assigned to the intermolecular CS state (neutral radical or radical dianion species) of **Fl-C18** in the supramolecular assembly. To directly observe the **Fl-C18** CS state, the ESR spectroscopy of the photo-irradiated **Fl-C18** at 173 K was performed. The ESR spectrum showed a clear signal corresponding to the **Fl-C18** radical at 3420 G (Figure S11).[51] Therefore, the CS state is generated in **Fl-C18**, which is critical in the switching of the photosensitizing mechanism via self-assembly.

The energy levels of the triplet and CS states of **Fl-C2** and **Fl-C18** were estimated using spectroscopic and electrochemical techniques to confirm our hypothesis. The phosphorescence spectra of **Fl-C2** and **Fl-C18** at 77 K are shown in Figure S12. The 0−0 bands of phosphorescence were observed at 621 and 626 nm for **Fl-C2** and **Fl-C18**, respectively, with energy levels of the triplet states of 2.0 eV for **Fl-C2** and **Fl-C18**. The energy levels of CS states were determined by electrochemical analysis (Figures S13 and S14) to be 1.6 and 1.3 eV for **Fl-C2** and **Fl-C18**, respectively. The energy level of the CS state is lower than that of the triplet state (Table 1). The proposed energy diagram of **Fl-C18** is shown in Figure S15. **Fl-C18** forms the $S_1$ state after photoirradiation and converted into the CS state directly or via a triplet state through SB−CS. Conversely, **Fl-C2** mainly loses the absorbed energy via fluorescence and proceeds via intersystem crossing to the triplet state.

**Table 1. Optical and Electrochemical Properties of Fl-C2 and Fl-C18**

| Compound | $E_{ox}$ (V vs Ag/AgCl) | $E_{red}$ (V vs Ag/AgCl) | $S_1$ (eV) | $T_1$ (eV) | $\Delta E_{cs}$ (eV) |
|---|---|---|---|---|---|
| Fl-C2 | 0.70 | −0.85 | 2.2 | 2.0 | 1.6 |
| Fl-C18 | 0.54 | −0.80 | 2.2 | 2.0 | 1.3 |

## 2.4. PDT Effects of Fl-C2 and Fl-C18

We investigated the potential of **Fl-C18** as an anticancer PDT. **Fl-C2** or **Fl-C18** and molecular probes (mitochondria and lysosome trackers) were incubated with PC9-luc cells (human adenocarcinoma lung cancer cells) with genes encoding firefly luciferase[52] to examine the cellular localization of **Fl-C2** and **Fl-C18**. Confocal laser scanning microscopy (CLSM) images are shown in Figure 6. The CLSM images of **Fl-C2** (100 nM)

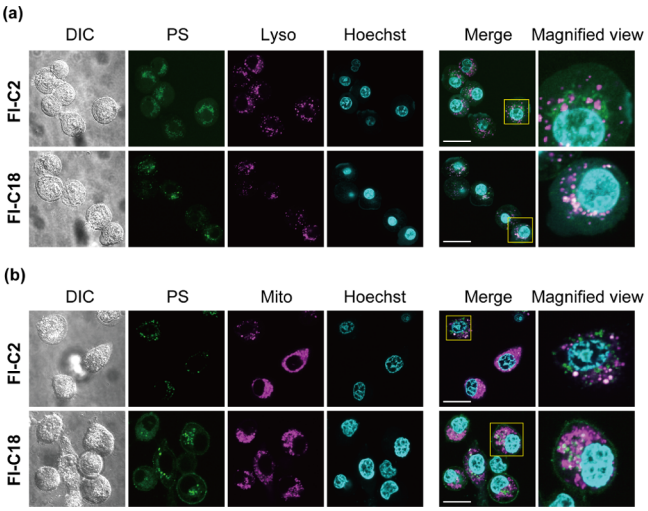


**Figure 6.** CLSM images of PC9-luc cells with (a) **Fl-C2**, **Fl-C18**, LysoTracker, and Hoechst and (b) **Fl-C2**, **Fl-C18**, MitoTracker, and Hoechst. The images show differential interference contrast, dye (**Fl-C2** or **Fl-C18**), tracker, Hoechst, merge, and the magnified view of merged images from left to right. Scale bar: 20 $\mu$m. Experimental conditions: [**Fl-C2**] = [**Fl-C18**] = 100 nM, [MitoTracker] = 250 nM, [LysoTracker] = 75 nM, and [Hoechst] = 500 nM, 37 °C.

and MitoTracker (250 nM) are well matched, indicating that **Fl-C2** localizes in mitochondria (Figure 6b). The CLSM images of **Fl-C18** (100 nM) and LysoTracker (75 nM) correspond, revealing **Fl-C18** localization in lysosomes (Figure 6a). Pearson correlation coefficients of **Fl-C2**/Lysotracker, **Fl-C2**/Lysotracker, **Fl-C18**/Mitotracker, and **Fl-C18**/Mitotracker images are summarized in Figure S16. The average Pearson correlation coefficients of **Fl-C2**/Lysotracker and **Fl-C18**/Lysotracker images are 0.39 and 0.64, respectively. The good correlation between **Fl-C18** and Lysotracker images indicates that **Fl-C18** tends to localize in lysosomes. The average Pearson correlation coefficients of **Fl-C2**/Mitotracker (0.79) and **Fl-C2**/Mitotracker (0.44) images also indicate the localization of **Fl-C2** in mitochondria. **Fl-C18** would enter cells via endocytosis and localize in the lysosomes. Indeed, dynasore, an inhibitor for clathrin-mediated endocytosis, decreased the mean fluorescence intensity of PC9-luc cells [dynasore(−): 1.05 × $10^4$, dynasore(+): 0.63 × $10^4$] (Figure S17). Lysosomes are an emerging target for PDT due to their close relationship with apoptosis and necrosis.[53,54] Both the localized organelles with the PSs (**Fl-C2**: mitochondria, **Fl-C18**: lysosome) are effective targets in PDT.[55] The cellular uptake of **Fl-C2** and **Fl-C18** after 12 h incubation (5.0 $\mu$M) was evaluated by Fl spectra. 20% **Fl-C2** and 9% **Fl-C18** entered the cells after incubation (Figure S18). The intracellular concentration of **Fl-C18** was estimated to 2.2-fold smaller than that of **Fl-C2**.



https://doi.org/10.1021/jacsau.2c00243
JACS Au 2022, 2, 1472−1478

Subsequently, the PDT effects of **Fl-C2** (1.0 $\mu$M) and **Fl-C18** (1.0 $\mu$M) were evaluated based on the luciferase activity of the PC9-luc cells (Figure 7). Without photoirradiation, the

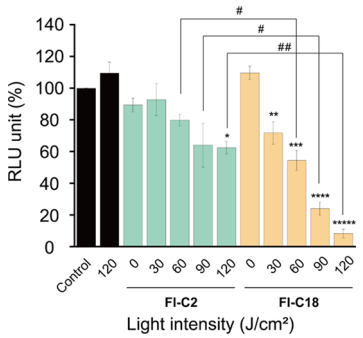


**Figure 7.** Luciferase activity in PC9-luc cells PDT-treated with **Fl-C2** and **Fl-C18** in relative light units: the activities decrease depending on the light irradiation [$n$ = 3, $^{*}p < 0.001$, $^{**}p < 0.05$, $^{***}p < 0.005$, $^{****}p < 0.0001$ vs control, $^{\#}p < 0.05$, $^{\#\#}p < 0.0005$ (two-tailed unpaired $t$-test)].

luciferase activities hardly decrease (**Fl-C2**: 89.4 ± 4.3%, **Fl-C18**: 109.7 ± 4.1%), indicating that these compounds show no cytotoxicity. In addition, photoirradiation of the PC9-luc cells without the PSs, using a high-power light-emitting diode (LED) at a wavelength of 490−500 nm (3 W cyan high-power LED, 10 min), also shows no cytotoxicity (109.5 ± 7.1%). **Fl-C2** and **Fl-C18** exhibited light-intensity-dependent PDT effects. After light irradiation (120 J/cm$^2$) of PC9-luc cells with **Fl-C2**, the luciferase activity decreased to 62.4 ± 3.9%. The rate of the decrease is light intensity-dependent, indicating the PDT effect of **Fl-C2** on the cells. The effect is insufficient and almost saturated at 90 J/cm$^2$ light intensity (luciferase activity: 64.1 ± 13.8%). Conversely, the PDT effect of **Fl-C18** increases depending on the power of light irradiation at ≤ 120 J/cm$^2$. After irradiation with 120 J/cm$^2$ light, the luciferase activity decreased to 8.3 ± 2.7%, indicating that most PC9-luc cells were dead. The CCK-8 assay of PC9-luc cells showed the same tendency with the luciferase assay (Figure S19). Under the hypoxic condition ($O_2$ concentration 2−5%), **Fl-C18** also showed a higher PDT effect than **Fl-C2**. The cell viability using **Fl-C2** and **Fl-C18** was 70 and 43% after photoirradiation (90 J/cm$^2$), respectively (Figure S20), under the $O_2$ depletion condition. The PDT effect of **Fl-C18** is significantly improved compared to that of **Fl-C2** under both normoxia and hypoxia conditions despite the low intracellular concentration. Although the localization organelles of **Fl-C2** and **Fl-C18** differ,[56] the significant improvement would be due to the change in the type of photosensitization reaction as **Fl-C18** functioned as a type I SPS in PC9-luc cells. Finally, we conformed the intracellular $O_2^{\bullet-}$ generation by **Fl-C2** and **Fl-C18** using dihydroethidium (**DHE**) which specifically detects of $O_2^{\bullet-}$ and hydrogen peroxide ($H_2O_2$).[57] The mean fluorescence intensity of the PC9-luc cells treated with **Fl-C18** (1.0 $\mu$M) was increased after photoirradiation (before: 2.44 × 10$^3$, after: 1.02 × 10$^4$) (Figure S21). This indicates that **Fl-C18** generated $O_2^{\bullet-}$ inside PC9-luc cells. On the other hand, in the case of **Fl-C2**, the mean fluorescence intensity was hardly changed after photoirradiation (before: 1.79 × 10$^3$, after: 1.27 × 10$^3$). These results support that **Fl-C2** and **Fl-C18** functioned as type II and type I PSs in the cells, respectively.

## 3. CONCLUSIONS

In this study, we proposed a development strategy for type I SPSs based on the induction of charge separation via self-assembly. Fluorescein, a conventional dye, functioned as a type II PS in the monomer state, with self-assembly switching the type of photosensitization observed. Spectroscopic and electrochemical analyses showed that the supramolecular assembly formed the CS state via photoirradiation, with the transition reasonable in terms of energy levels. Furthermore, **Fl-C18** showed a light-intensity-dependent PDT effect on human adenocarcinoma lung cancer cells, which was sufficiently improved compared with that of **Fl-C2**. As there are numerous molecules that exhibit the potential to form a CS state during assembly, molecules without type I photosensitizing properties in the monomer state may function as type I SPSs. This phenomenon implies that various organic dyes function as a type I PS by simple self-assembly. This strategy using the CS state for the development of a type I PS may be applied not only in supramolecular assembly but also in monomeric organic PSs. This study provides a novel strategy for developing type I SPSs and contributes to efficient PDT.

## ■ ASSOCIATED CONTENT

### Supporting Information

The Supporting Information is available free of charge at https://pubs.acs.org/doi/10.1021/jacsau.2c00243.

Materials, experimental methods, synthetic procedures, characterization data, and photophysical and electrochemical data (PDF)

## ■ AUTHOR INFORMATION


### Corresponding Authors

**Hajime Shigemitsu** − *Department of Applied Chemistry, Graduate School of Engineering, Osaka University, Suita 565-0871, Japan; Frontier Research Base for Global Young Researchers, Graduate School of Engineering, Integrated Frontier Research for Medical Science Division, Institute for Open and Transdisciplinary Research Initiatives (OTRI), and Global Center for Medical Engineering and Informatics, Osaka University, Suita 565-0871, Japan;* orcid.org/0000-0002-3104-049X; Email: shigemitsu@chem.eng.osaka-u.ac.jp

**Toshiyuki Kida** − *Department of Applied Chemistry, Graduate School of Engineering, Osaka University, Suita 565-0871, Japan; Integrated Frontier Research for Medical Science Division, Institute for Open and Transdisciplinary Research Initiatives (OTRI), Osaka University, Suita 565-0871, Japan;* orcid.org/0000-0002-5777-8580; Email: kida@chem.eng.osaka-u.ac.jp

### Authors

**Kei Ohkubo** − *Institute for Advanced Co-creation Studies, Osaka University, Suita, Osaka 565-0871, Japan;* orcid.org/0000-0001-8328-9249

**Kazuhide Sato** − *Department of Respiratory Medicine, Nagoya University Graduate School of Medicine, Nagoya, Aichi 466-8550, Japan; Institute for Advanced Research, Nagoya University, Nagoya, Aichi 464-0814, Japan;* orcid.org/0000-0003-3025-088X




https://doi.org/10.1021/jacsau.2c00243
JACS Au 2022, 2, 1472−1478

**Asuka Bunno** − *Department of Applied Chemistry, Graduate School of Engineering, Osaka University, Suita 565-0871, Japan*

**Tadashi Mori** − *Department of Applied Chemistry, Graduate School of Engineering, Osaka University, Suita 565-0871, Japan;* orcid.org/0000-0003-3918-0873

**Yasuko Osakada** − *Institute for Advanced Co-creation Studies, Osaka University, Suita, Osaka 565-0871, Japan; The Institute of Scientific and Industrial Research (ISIR), Osaka University, Ibaraki, Osaka 567-0047, Japan;* orcid.org/0000-0003-4078-0112

**Mamoru Fujitsuka** − *The Institute of Scientific and Industrial Research (ISIR), Osaka University, Ibaraki, Osaka 567-0047, Japan;* orcid.org/0000-0002-2336-4355

Complete contact information is available at: https://pubs.acs.org/10.1021/jacsau.2c00243

### Notes

The authors declare no competing financial interest.

## ■ ACKNOWLEDGMENTS

This work was performed at Osaka University and financially supported by a grant-in-aid for Young Scientists (JSPS KAKENHI Grant no. JP18K14189 and 21K14601), AMED (grant nos. JP19lm0203007 and JP19lm0203014), the Takeda Science Foundation, the Kowa Life Science Foundation, the Senri Life Science Foundation, and the Kato Memorial Bioscience Foundation. We appreciate Y. Murakami for technical support for TEM observation. We also thank Dr. Y. Morimoto and Dr. K. Oohora for technical support for ESR measurement. Finally, we appreciate Dr. T. Nakagawa for kind support for measurement of transition absorption spectra.

## ■ ABBREVIATIONS

| | |
|---|---|
| PDT | photodynamic therapy |
| ROS | reactive oxygen species |
| PS | photosensitizer |
| SPS | supramolecular photosensitizer |
| CS | charge separated |
| SB−CS | symmetry-breaking charge separation |
| DMSO | dimethylsulfoxide |
| DLS | dynamic light scattering |
| TEM | transmission electron microscopy |
| ABDA | 9,10-anthracenediyl-bis(methylene)-dimalonic acid |
| DHR123 | dihydrorhodamine 123 |
| Rh123 | rhodamine123 |
| 4-OH-TEMP | 4-hydroxy-2,2,6,6-tetramethylpiperidine |
| CPH | 1-hydroxy-3-carboxy-2,2,5,5-tetramethylpyrrolidine |
| 4-OH-TEMPO | 4-hydroxy-2,2,6,6-tetramethylpiperidine 1-oxyl |
| ESR | electron spin resonance |
| SOD | superoxide dismutase |
| CLSM | confocal laser microscopy |
| DHE | dihydroethidium |

## ■ REFERENCES

(1) Dolmans, D. E. J. G. J.; Fukumura, D.; Jain, R. K. Photodynamic therapy for cancer. *Nat. Rev. Cancer* **2003**, *3*, 380−387.

(2) Castano, A. P.; Mroz, P.; Hamblin, M. R. Photodynamic therapy and anti-tumour immunity. *Nat. Rev. Cancer* **2006**, *6*, 535−545.

(3) Celli, J. P.; Spring, B. Q.; Rizvi, I.; Evans, C. L.; Samkoe, K. S.; Verma, S.; Pogue, B. W.; Hasan, T. Imaging and photodynamic therapy: Mechanisms, monitoring, and optimization. *Chem. Rev.* **2010**, *110*, 2795−2838.

(4) Fan, W.; Huang, P.; Chen, X. Overcoming the Achilles' heel of photodynamic therapy. *Chem. Soc. Rev.* **2016**, *45*, 6488−6519.

(5) Juarranz, Á.; Jaén, P.; Sanz-Rodríguez, F.; Cuevas, J.; González, S. Photodynamic therapy of cancer. Basic principles and applications. *Clin. Transl. Oncol.* **2008**, *10*, 148−154.

(6) Lovell, J. F.; Liu, T. W. B.; Chen, J.; Zheng, G. Activatable photosensitizers for imaging and therapy. *Chem. Rev.* **2010**, *110*, 2839−2857.

(7) Zhao, X.; Liu, J.; Fan, J.; Chao, H.; Peng, X. Recent progress in photosensitizers for overcoming the challenges of photodynamic therapy: from molecular design to application. *Chem. Soc. Rev.* **2021**, *50*, 4185−4219.

(8) Zhang, W.; Huo, F.; Cheng, F.; Yin, C. Employing an ICT-FRET Integration Platform for the Real-Time Tracking of SO2 Metabolism in Cancer Cells and Tumor Models. *J. Am. Chem. Soc.* **2020**, *142*, 6324−6331.

(9) Pervaiz, S.; Olivo, M. Art and science of photodynamic therapy. *Clin. Exp. Pharmacol. Physiol.* **2006**, *33*, 551−556.

(10) Dougherty, T. J.; Gomer, C. J.; Henderson, B. W.; Jori, G.; Kessel, D.; Korbelik, M.; Moan, J.; Peng, Q. Photodynamic therapy. *J. Natl. Cancer Inst.* **1998**, *90*, 889−905.

(11) Baptista, M. S.; Cadet, J.; Di Mascio, P.; Ghogare, A. A.; Greer, A.; Hamblin, M. R.; Lorente, C.; Nunez, S. C.; Ribeiro, M. S.; Thomas, A. H.; Vignoni, M.; Yoshimura, T. M. Type I and type II photosensitized oxidation reactions: guidelines and mechanistic pathways. *Photochem. Photobiol.* **2017**, *93*, 912−919.

(12) Li, M.; Xia, J.; Tian, R.; Wang, J.; Fan, J.; Du, J.; Long, S.; Song, X.; Foley, J. W.; Peng, X. Near-infrared light-initiated molecular superoxide radical generator: Rejuvenating photodynamic therapy against hypoxic tumors. *J. Am. Chem. Soc.* **2018**, *140*, 14851−14859.

(13) Liu, J.-n.; Bu, W.; Shi, J. Chemical Design and Synthesis of Functionalized Probes for Imaging and Treating Tumor Hypoxia. *J. Chem. Rev.* **2017**, *117*, 6160−6224.

(14) Zhou, Z.; Song, J.; Nie, L.; Chen, X. Reactive oxygen species generating systems meeting challenges of photodynamic cancer therapy. *Chem. Soc. Rev.* **2016**, *45*, 6597−6626.

(15) Loftus, L. M.; Al-Afyouni, K. F.; Rohrabaugh, T. N., Jr; Gallucci, J. C.; Moore, C. E.; Rack, J. J.; Turro, C. Unexpected Role of Ru(II) Orbital and Spin Contribution on Photoinduced Ligand Exchange: New Mechanism To Access the Photodynamic Therapy Window. *J. Phys Chem. Chem. C* **2019**, *123*, 10291−10299.

(16) Li, X.; Lee, S.; Yoon, J. Supramolecular photosensitizers rejuvenate photodynamic therapy. *Chem. Soc. Rev.* **2018**, *47*, 1174−1188.

(17) Xie, Z.; Fan, T.; An, J.; Choi, W.; Duo, Y.; Ge, Y.; Zhang, B.; Nie, G.; Xie, N.; Zheng, T.; Chen, Y.; Zhang, H.; Kim, J. S. Emerging combination strategies with phototherapy in cancer nanomedicine. *Chem. Soc. Rev.* **2020**, *49*, 8065−8087.

(18) Kwon, N.; Kim, H.; Li, X.; Yoon, J. Supramolecular agents for combination of photodynamic therapy and other treatments. *Chem. Sci.* **2021**, *12*, 7248−7268.

(19) Sun, L.; Wang, J.; Yang, B.; Wang, X.; Yang, G.; Wang, X.; Jiang, Y.; Wang, T.; Jiang, J. Assembled small organic molecules for photodynamic therapy and photothermal therapy. *RSC Adv.* **2021**, *11*, 10061−10074.

(20) Zou, Q.; Abbas, M.; Zhao, L.; Li, S.; Shen, G.; Yan, X. Biological photothermal nanodots based on self-assembly of peptide−porphyrin conjugates for antitumor therapy. *J. Am. Chem. Soc.* **2017**, *139*, 1921−1927.

(21) Zhu, H.; Wang, H.; Shi, B.; Shangguan, L.; Tong, W.; Yu, G.; Mao, Z.; Huang, F. Supramolecular peptide constructed by molecular Lego allowing programmable self-assembly for photodynamic therapy. *Nat. Commun.* **2019**, *10*, 2412.

(22) Webber, M. J.; Langer, R. Drug delivery by supramolecular design. *Chem. Soc. Rev.* **2017**, *46*, 6600−6620.

(23) Sato, K.; Hendricks, M. P.; Palmer, L. C.; Stupp, S. I. Peptide supramolecular materials for therapeutics. *Chem. Soc. Rev.* **2018**, *47*, 7539−7551.
(24) Cheetham, A. G.; Chakroun, R. W.; Ma, W.; Cui, H. Self-assembling prodrugs. *Chem. Soc. Rev.* **2017**, *46*, 6638−6663.
(25) Shigemitsu, H.; Hamachi, I. Supramolecular assemblies responsive to biomolecules toward biological applications. *Chem.—Asian J.* **2015**, *10*, 2026−2038.
(26) Busseron, E.; Ruff, Y.; Moulin, E.; Giuseppone, N. Supramolecular self-assemblies as functional nanomaterials. *Nanoscale* **2013**, *5*, 7098−7140.
(27) Hu, F.; Mao, D.; Kenry; Cai, X.; Wu, W.; Kong, D.; Liu, B. A Light-Up Probe with Aggregation-Induced Emission for Real-Time Bio-orthogonal Tumor Labeling and Image-Guided Photodynamic Therapy. *Angew. Chem., Int. Ed.* **2018**, *57*, 10182−10186.
(28) Li, Q.; Li, Y.; Min, T.; Gong, J.; Du, L.; Phillips, D. L.; Liu, J.; Lam, J. W. Y.; Sung, H. H. Y.; Williams, I. D.; Kwok, R. T. K.; Ho, C. L.; Li, K.; Wang, J.; Tang, B. Z. Time-Dependent Photodynamic Therapy for Multiple Targets: A Highly Efficient AIE-Active Photosensitizer for Selective Bacterial Elimination and Cancer Cell Ablation. *Angew. Chem., Int. Ed.* **2020**, *59*, 9470−9477.
(29) Ji, C.; Gao, Q.; Dong, X.; Yin, W.; Gu, Z.; Gan, Z.; Zhao, Y.; Yin, M. A Size-Reducible Nanodrug with an Aggregation-Enhanced Photodynamic Effect for Deep Chemo-Photodynamic Therapy. *Angew. Chem., Int. Ed.* **2018**, *57*, 11384−11388.
(30) Li, X.; Lee, D.; Huang, J.-D.; Yoon, J. Phthalocyanine-assembled nanodots as photosensitizers for highly efficient type I photoreactions in photodynamic therapy. *Angew. Chem., Int. Ed.* **2018**, *57*, 9885−9890.
(31) Chen, D.; Xu, Q.; Wang, W.; Shao, J.; Huang, W.; Dong, X. Type I photosensitizers revitalizing photodynamic oncotherapy. *Small* **2021**, *17*, 2006742.
(32) Ding, H.; Yu, H.; Dong, Y.; Tian, R.; Huang, G.; Boothman, D. A.; Sumer, B. D.; Gao, J. Photoactivation switch from type II to type I reactions by electron-rich micelles for improved photodynamic therapy of cancer cells under hypoxia. *J. Controlled Release* **2011**, *156*, 276−280.
(33) Zhuang, Z.; Dai, J.; Yu, M.; Li, J.; Shen, P.; Hu, R.; Lou, X.; Zhao, Z.; Tang, B. Z. Type I photosensitizers based on phosphindole oxide for photodynamic therapy: apoptosis and autophagy induced by endoplasmic reticulum stress. *Chem. Sci.* **2020**, *11*, 3405−3417.
(34) Shigemitsu, H.; Tani, Y.; Tamemoto, T.; Mori, T.; Li, X.; Osakada, Y.; Fujitsuka, M.; Kida, T. Aggregation-induced photocatalytic activity and efficient photocatalytic hydrogen evolution of amphiphilic rhodamines in water. *Chem. Sci.* **2020**, *11*, 11843−11848.
(35) Shigemitsu, H.; Tamemoto, T.; Ohkubo, K.; Mori, T.; Osakada, Y.; Fujitsuka, M.; Kida, T. A cyanine dye based supramolecular photosensitizer enabling visible-light-driven organic reaction in water. *Chem. Commun.* **2021**, *57*, 11217−11220.
(36) Tanaka, K.; Miura, T.; Umezawa, N.; Urano, Y.; Kikuchi, K.; Higuchi, T.; Nagano, T. Rational design of fluorescein-based fluorescence probes. Mechanism-based design of a maximum fluorescence probe for singlet oxygen. *J. Am. Chem. Soc.* **2001**, *123*, 2530−2536.
(37) Park, S.-H.; Kwon, N.; Lee, J.-H.; Yoon, J.; Shin, I. Synthetic ratiometric fluorescent probes for detection of ions. *Chem. Soc. Rev.* **2020**, *49*, 143−179.
(38) Surrey, T.; Elowitz, M. B.; Wolf, P.-E.; Yang, F.; Nédélec, F.; Shokat, K.; Leibler, S. Chromophore-assisted light inactivation and self-organization of microtubules and motors. *Proc. Natl. Acad. Sci. U.S.A.* **1998**, *95*, 4293−4298.
(39) Jacobson, K.; Rajfur, Z.; Vitriol, E.; Hahn, K. Chromophore-assisted laser inactivation in cell biology. *Trends Cell Biol.* **2008**, *18*, 443−450.
(40) Paziewske-Nowak, A.; Dawgul, M.; Pijanowska, D. G. Comparative Study on Voltammetric and Spectrofluorimetric Methods for Fluorescein Detection. *Int. J. Electrochem. Sci.* **2019**, *14*, 3764−3776.
(41) Das, S.; Chattopadhyay, A. P.; De, S. Controlling J aggregation in fluorescein by bile salt hydrogels. *J. Photochem. Photobiol. A: Chem.* **2008**, *197*, 402−414.
(42) Entradas, T.; Waldron, S.; Volk, M. The detection sensitivity of commonly used singlet oxygen probes in aqueous environments. *J. Photochem. Photobiol. B: Biol.* **2020**, *204*, 111787.
(43) Kiani-Esfahani, A.; Tavalaee, M.; Deemeh, M. R.; Hamiditabar, M.; Nasr-Esfahani, M. H. DHR123: an alternative probe for assessment of ROS in human spermatozoa. *Syst. Biol. Reprod. Med.* **2012**, *58*, 168−74.
(44) Abreu, I. A.; Cabelli, D. E. Superoxide dismutases -a review of the metal-associated mechanistic variations. *Biochim. Biophys. Acta* **2010**, *1804*, 263−274.
(45) Crack, J. C.; Green, J.; Cheesman, M. R.; Le Brun, N. E.; Thomson, A. J. Superoxide-mediated amplification of the oxygen-induced switch from [4Fe-4S] to [2Fe-2S] clusters in the transcriptional regulator FNR. *Proc. Natl. Acad. Sci. U.S.A.* **2007**, *104*, 2092−2097.
(46) Lion, Y.; Gandin, E.; Vorst, A. On the production of nitroxide radicals by singlet oxygen reaction: An EPR study. *Photochem. Photobiol.* **1980**, *31*, 305−309.
(47) Dikalov, S.; Skatchkov, M.; Bassenge, E. Spin trapping of superoxide radicals and peroxynitrite by 1-hydroxy-3-carboxy-pyrrolidine and 1-hydroxy-2,2,6,6-tetramethyl-4-oxo-piperidine and the stability of corresponding nitroxyl radicals towards biological reductants. *Biochem. Biophys. Res. Commun.* **1997**, *231*, 701−704.
(48) Nakagawa, T.; Okamoto, K.; Hanada, H.; Katoh, R. Probing with randomly interleaved pulse train bridges the gap between ultrafast pump-probe and nanosecond flash photolysis. *Opt. Lett.* **2016**, *41*, 1498−1501.
(49) Song, L.; Varma, C. A.; Verhoeven, J. W.; Tanke, H. J. Influence of the triplet excited state on the photobleaching kinetics of fluorescein in microscopy. *Biophys. J.* **1996**, *70*, 2959−2968.
(50) Kasche, V.; Lindqvist, L. Reactions between the Triplet State of Fluorescein and Oxygen. *J. Phys. Chem.* **1964**, *68*, 817−823.
(51) Shigeya, N.; Yoshiharu, S.; Shiro, K.; Hiroshi, K. ESR study on fluorescein semiquinone radical. *Bull. Chem. Soc. Jpn.* **1974**, *47*, 2121−2125.
(52) Yasui, H.; Nishinaga, Y.; Taki, S.; Takahashi, K.; Isobe, Y.; Shimizu, M.; Koike, C.; Taki, T.; Sakamoto, A.; Katsumi, K.; Ishii, K.; Sato, K. Near-infrared photoimmunotherapy targeting GPR87: Development of a humanised anti-GPR87 mAb and therapeutic efficacy on a lung cancer mouse model. *EBioMedicine* **2021**, *67*, 103372.
(53) Tsubone, T. M.; Martins, W. K.; Pavani, C.; Junqueira, H. C.; Itri, R.; Baptista, M. S. Enhanced efficiency of cell death by lysosome-specific photodamage. *Sci. Rep.* **2017**, *7*, 6734.
(54) Zhou, Z.; Liu, J.; Huang, J.; Rees, T. W.; Wang, Y.; Wang, H.; Li, X.; Chao, H.; Stang, P. J. A self-assembled Ru−Pt metallacage as a lysosome-targeting photosensitizer for 2-photon photodynamic therapy. *Proc. Natl. Acad. Sci. U.S.A.* **2019**, *116*, 20296−20302.
(55) Mahalingam, S. M.; Ordaz, J. D.; Low, P. S. Targeting of a photosensitizer to the mitochondrion enhances the potency of photodynamic therapy. *ACS Omega* **2018**, *3*, 6066−6074.
(56) Li, X.; Zhao, Y.; Zhang, T.; Xing, D. Mitochondria-specific agents for photodynamic cancer therapy: A key determinant to boost the efficacy. *Adv. Healthc. Mater.* **2021**, *10*, 2001240.
(57) Chen, J.; Rogers, S. C.; Kavdia, M. Analysis of kinetics of dihydroethidium fluorescence with superoxide using xanthine oxidase and hypoxanthine assay. *Ann. Biomed. Eng.* **2013**, *41*, 327−337.


https://doi.org/10.1021/jacsau.2c00243
*JACS Au* 2022, 2, 1472−1478